

Review Paper

Homogeneous Ice Nucleation in Water and Aqueous Solutions

By Thomas Koop*

University of Bielefeld, Faculty of Chemistry, Universitätsstraße 25, D-33615 Bielefeld, Germany

(Received August 17, 2004; accepted August 25, 2004)

Ice Nucleation / Metastable Water / Supercooled Aqueous Solutions / Water Activity

This review provides an introduction to ice nucleation processes in supercooled water and aqueous solutions. Concepts for experimental techniques suitable to study homogeneous ice nucleation are addressed, in particular differential scanning calorimetry of inverse emulsions. Ice nucleation data from aqueous solutions have been analyzed using two approaches, and the interrelations between those are examined. It is argued that the ice nucleation process is driven entirely by thermodynamic quantities and how this can be understood in the context of three proposed theories for supercooled liquid water. Ice nucleation data for pure water droplets surrounded by a gas have been compiled and evaluated; within experimental uncertainty neither a volume dependent nucleation process nor a surface dependent nucleation process is convincingly supported by the analysis. Finally, open questions in the area of supercooled aqueous solutions and ice nucleation are discussed.

1. Introduction

The properties of liquid water are highly anomalous when compared to most other liquids. The cause for the exceptional behavior of liquid water are the properties of its molecular building block, the H₂O molecule. Water molecules interact with each other through hydrogen bonds, thereby forming an open network structure with local tetrahedral symmetry. Most observable features of water are a direct result of the attraction between water molecules in the hydrogen bonding network under different external conditions. Probably the best

* E-mail: thomas.koop@uni-bielefeld.de

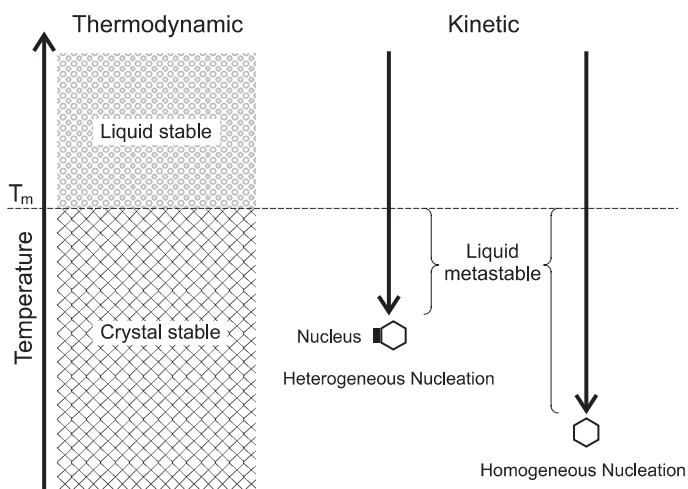


Fig. 1. Schematic picture comparing different nucleation mechanisms for the freezing of a liquid. T_m is the melting point of the crystalline phase.

known of water's anomalies is its density maximum at 277 K, a fact recognized already more than three hundred years ago [1]. Another peculiarity is that water expands when it freezes: ice has a smaller density than liquid water, which is why ice floats on lakes and in a gin tonic. The transformation of liquid water to ice has fascinated scientists for centuries [2]. We know today that water does not necessarily freeze at its equilibrium melting point, but can be cooled to temperatures considerably below 273.15 K. Since the supercooling of water and aqueous solutions is the central theme of this review, we first define the basic terminology of supercooled liquids.

All liquids can be cooled below their equilibrium melting point, T_m [3]. The temperature of T_m is defined by thermodynamics as the temperature where the liquid and crystalline phases can coexist in equilibrium with each other. Above T_m the liquid is the stable phase, below T_m the crystal is the stable phase (left panel of Fig. 1). A liquid at internal thermodynamic equilibrium below T_m is in a metastable state. Here, metastable means that the liquid assumes a local minimum in the Gibbs free energy landscape. The absolute minimum corresponds to the stable crystalline state.

The temperature at which freezing actually occurs in real samples is determined by kinetics and involves a nucleation process. Typically, the nucleation of the crystalline phase is initiated at the surface of a solid nucleus present in the liquid (middle panel in Fig. 1). For example, in chemistry laboratory courses it is common practise to initiate crystallization of a supercooled solution by scratching the surface of the glass container with a sharp-edged rod. This releases tiny glass particles which serve as nuclei for the crystallization. On the other hand, a liquid devoid of any nuclei can also nucleate sponta-

neously by forming a stable germ through internal fluctuations. This process is called homogeneous nucleation, while crystallization initiated by nuclei is called heterogeneous nucleation. Under otherwise identical conditions heterogeneous nucleation always occurs at a higher temperature than homogeneous nucleation. This is generally true because the addition of foreign nuclei to a liquid can only enhance the overall nucleation probability. Hence, homogeneous nucleation serves as the lower temperature limit to which a liquid can be supercooled without freezing. The temperature at which heterogeneous nucleation occurs depends strongly on the suitability of a particular nucleus to induce nucleation. In contrast, the homogeneous nucleation temperature, T_f , is a genuine property of the metastable liquid itself. The homogeneous ice nucleation temperature of micrometer-sized samples of pure water is $T_f \simeq 235$ K. Heterogeneous ice nucleation can occur anywhere between T_m and T_f , thereby controlling the observed magnitude of supercooling. The ability of water to supercool has been known for quite some time and its relevance in atmospheric processes has been recognized with the advent of modern meteorology. The earliest records of supercooled water are most likely the experiments by Daniel Fahrenheit of March 2–4, 1721 [4], in which he observed that water droplets in an evacuated glass bulb remained liquid to temperatures of about 264 K. Almost two centuries later, much larger supercooling was possible with the development of Wilson's expansion chamber [5], enabling Cwiling in 1947 to observe small water droplets to freeze at about 232 K [6]. At the same time, Schaefer independently invented a cold box technique and concluded from his measurements that freezing of small water drops occurs at about 234 K [7, 8]. From today's perspective it appears that Cwiling and Schaefer were the first to supercool water to the homogeneous ice nucleation limit.

2. Theories of liquid water

At an ambient pressure of 1 bar, liquid water comes about in a number of forms (Fig. 2). We have already discussed the existence of stable water above T_m and metastable water between T_m and T_f . Crystallization at T_f can be avoided by hyperquenching liquid water at extremely high cooling rates $\gtrsim 10^5$ K s⁻¹ to temperatures below 100 K [9]. This procedure results in an amorphous form of water, a glass. When glassy water is reheated, it undergoes a glass transition at about 130 K,¹ thereby forming ultraviscous water, which crystallizes upon further warming at about 150 K. The region between T_f and T_x is called “no man's land” because it is not accessible on experimen-

¹ It has been suggested that T_g of water and very dilute aqueous solutions should be at around 165 ± 5 K based on comparison with other network-forming liquids; however, this transition cannot be measured directly since water crystallizes upon warming at about 150–160 K [10, 11].

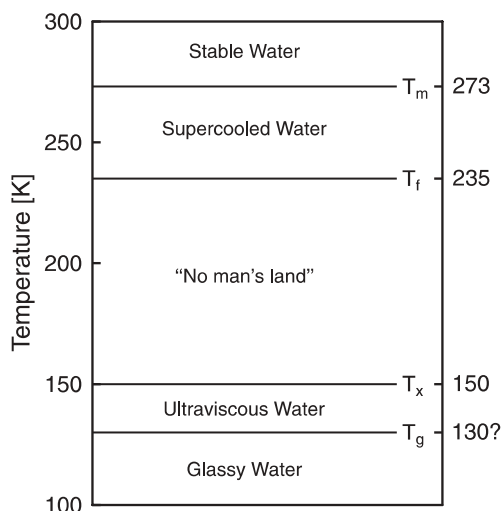


Fig. 2. Schematic illustration of different domains of condensed non-crystalline H_2O at atmospheric pressure (adapted with changes from Ref. [1]). The domain above T_m is stable; all others are metastable. T_m denotes the melting temperature of hexagonal ice, T_f the homogeneous nucleation temperature of micrometer-sized water droplets, T_x the crystallization temperature of ultraviscous water upon warming, and T_g the glass transition temperature. The region between T_f and T_x is termed “no-man’s-land”, as experiments on the liquid phase cannot be performed. Indicated on the right axis are the experimentally observed transformation temperatures of the different forms. The temperature associated with T_g is currently being discussed, see footnote 1.

tal time scales due to rapid crystallization of ice in this temperature range (see Fig. 2).

At higher pressures the picture becomes more complicated. Two distinct amorphous forms of water have been discovered, low density amorphous water (LDA) and high density amorphous water (HDA). At low temperatures the two can be interconverted by changing the applied mechanical pressure in a so-called polyamorphic transition [12]. Several thermodynamic parameters, *e.g.*, molar volume, undergo surprisingly sharp changes during this transformation, similar to those in a first-order phase transition. Numerous other experimental observations of water at low temperatures exist and the picture of how the different properties are connected is very complex [1, 13].

Currently, there are three hypotheses to explain the properties of water in the supercooled metastable range [1, 13, 14]. The first is the so-called stability-limit hypothesis [15, 16]. It is based on early observations showing that various properties of supercooled water such as the heat capacity seem to diverge to infinity at about 228 K [17]. This apparent singularity at ambient pressure is proposed to be just one point on a spinodal temperature line (T_s , dotted line in Fig. 3(a)). A spinodal line separates metastable and unstable states. Thus liquid

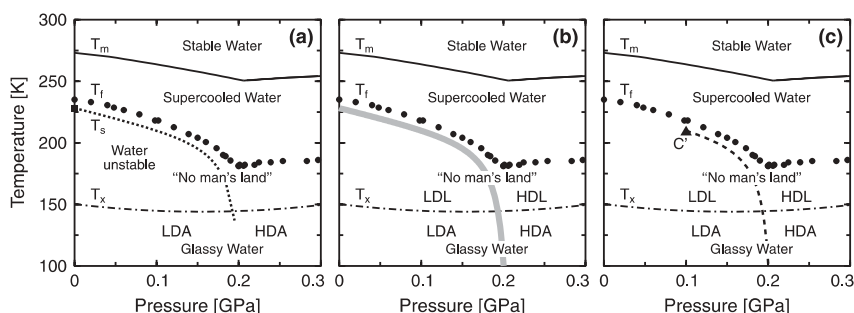


Fig. 3. Schematic representation of the three currently discussed competing theories describing the behavior of liquid water (after Ref. [1]): (a) the stability limit hypothesis; (b) the singularity-free hypothesis; and (c) the liquid-liquid critical point hypothesis. The location of T_m , T_f , and T_x as a function of pressure is indicated by the solid lines, circles, and dash-dotted lines, respectively. The glass temperatures T_g are not shown but are expected to be somewhere below T_x line. LDA and HDA indicate the regions where the two amorphous forms are observed. In (a), the dotted T_s line represents the spinodal line with the square indicating $T_s = 228$ K at ambient pressure. In (b), the grey line indicates the locus of maximum changes in thermodynamic properties. C' in panel (c) denotes the proposed second critical point of water, with a coexistence line (dashed) separating the two liquid forms of water, LDL and HDL.

water becomes unstable at temperatures below T_s , that is, it cannot exist under these conditions. Therefore, in this picture, LDA and ultraviscous water are thought to represent another form of water (sometimes called water II) different from normal water above T_s . Experimental data in support of the stability limit hypothesis are constrained to temperatures above T_f , which is several kelvins above the speculated location of T_s . It is therefore possible that some thermodynamic functions increase rapidly close to T_s , however, without a singularity. Exactly this behavior is predicted by the second theory, the singularity-free hypothesis (Fig. 3(b)). This theory suggests strong changes in thermodynamical properties near T_f , but with a thermodynamic continuity between liquid water above and below T_f [18, 19]. Similarly, the polyamorphic transition between LDA and HDA is considered to be a consequence of relaxation phenomena that resemble features of a genuine phase transition, but are not. Finally, the third suggestion (Fig. 3(c)) is the liquid-liquid phase transition hypothesis [20, 21]. This theory proposes the existence of a second critical point of water, at which the liquid phase separates into two distinct liquid phases, a low density liquid (LDL) and a high density liquid (HDL). This theory suggests that LDL and HDL resemble the liquid forms of the observed amorphous states LDA and HDA. The locus of the second critical point is assumed to be below T_f at a pressure of about 0.1 GPa, somewhere in no man's land. This is why it is difficult to test experimentally which of the three theories is correct.

Several experimental studies exist that support either theory indirectly. Mishima and Suzuki have presented Raman spectroscopic studies on the HDA-

to-LDA transition that are in support of the liquid–liquid critical point theory [22]. Also, observations of low temperature metastable melting curves of various H_2O and D_2O ices seem to support the second critical point hypothesis [23, 24]. The opposite is true for the recent discovery of a new very dense amorphous form of water called very-high density amorphous ice, VHDA [25, 26]. In addition, several intermediate structures were observed in neutron diffraction studies with a gradual change from HDA to LDA [27]. The latter studies may alter predictions for the location of the second critical point and may even call the liquid–liquid critical point theory into question [28]. On the other hand, these measurements are in agreement with model simulations, which suggest that water may exhibit multiple liquid–liquid phase transitions [29].

It is important to note that both the singularity-free scenario and the liquid–liquid critical point scenario suggest a thermodynamic continuity between liquid water and LDA at ambient pressure. This is supported by neutron diffraction measurements which show that the structure of liquid water changes towards the LDA structure when cooled at ambient pressure [30, 31]. Also, liquid water that is cooled rapidly at 1 bar becomes LDA. Finally, other measurements show that small water clusters consisting of a few thousand molecules can be supercooled to temperatures below T_s before they freeze [32–36]. However, care should be taken in the interpretation of these experiments, because clusters of such small size are subject to large internal pressures due to the Kelvin effect.

This review is mainly concerned with the behavior of supercooled aqueous solutions. It is therefore of interest to discuss the possible implications of the theories of supercooled liquid water for our understanding of supercooled aqueous solutions at low temperatures. For illustrative purposes, the $\text{H}_2\text{SO}_4/\text{H}_2\text{O}$ -phase diagram is shown in Fig. 4 using the same notation as for pure water at ambient pressure (see Fig. 2). Both T_m and T_f decrease strongly with increasing concentration. On the other hand, T_x and T_g increase with increasing concentration. The region of no man's land, encompassed by the T_f and T_x lines, is not accessible on experimental timescales. However, with careful sample preparation, some properties in the supercooled and glassy states can be tested experimentally. For example, the dissociation equilibrium of the bisulfate ion $\text{HSO}_4^-(\text{aq}) \rightleftharpoons \text{H}^+(\text{aq}) + \text{SO}_4^{2-}(\text{aq})$ has been studied with Raman spectroscopy in the supercooled state between T_m and T_f [37, 38] and in the glassy state below T_g [39].

Some properties of supercooled water (for example heat capacities) undergo changes upon the addition of solutes that are similar to those when pressure is applied to pure water [40]. Such observations suggest that scenarios similar to those proposed for pure water (Fig. 3) might also be applicable in explaining the behavior of aqueous solutions supercooled with respect to ice. Data presented below indeed point in this direction.

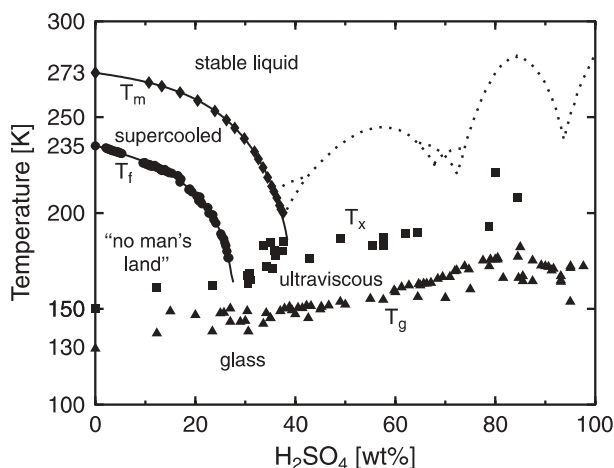


Fig. 4. The binary $\text{H}_2\text{SO}_4/\text{H}_2\text{O}$ phase diagram together with the different transition temperatures as defined for pure water in Fig. 2. The melting temperatures of ice (T_m , diamonds) and the various hydrates (dotted lines) have been taken from [108]. Also shown are the T_f values as circles [52], T_x data as squares [109–112], and T_g data as triangles [111, 113, 114].

3. Experimental techniques

3.1 General concept

Measurements on supercooled water are difficult to perform because of the likelihood of ice nucleation to occur in samples of normal size and purity [17]. As pointed out above all ice nuclei have to be removed from a sample in order to study homogeneous ice nucleation. This is a notoriously difficult task since even a single ice nucleus can initiate heterogeneous nucleation, thereby triggering the freezing of the entire sample (see Fig. 5(a)). One strategy to prepare liquid samples devoid of any ice nuclei is dividing a bulk sample into numerous small samples. As a result, only a minor fraction of the small samples contain ice nuclei while most of the others are free of them (Fig. 5(b)). Therefore, only a small number of samples freeze heterogeneously, but the majority of the samples freezes homogeneously.

Several experimental techniques exist that make use of the concept described in Fig. 5. In the 1960s many experimental studies on properties of water in the supercooled state were performed using water samples contained in small capillaries [17]. First experiments on inverse (water-in-oil) emulsions were performed in the 1940s and 50s [41, 42] and the emulsion technique was perfected subsequently [43, 44], allowing to supercool water to 235 K. The most recent experimental studies on ice nucleation rate coefficients in supercooled water involve expansion chambers of various sizes [45, 46], elec-

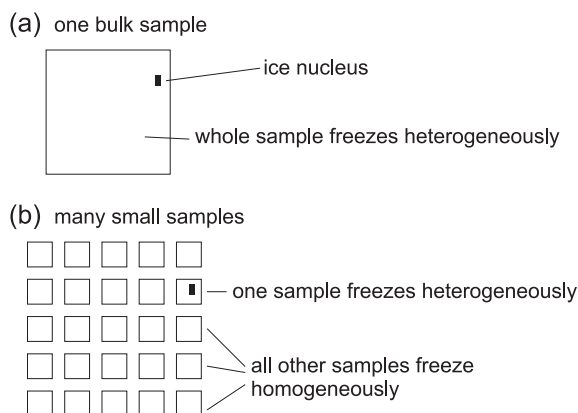


Fig. 5. Comparison between bulk and small sample freezing experiments. The effect of ice nuclei can be minimized by dispersing a bulk sample into numerous small samples. As a result, homogeneous nucleation is allowed to occur in a major fraction of the samples.

trodynamic balance experiments [47, 48], optical microscopy [49], and droplet train tubes [50].

Experimental investigations of ice nucleation in supercooled aqueous solutions are much more recent than studies on pure water. The breakthrough in this field came with the advent of emulsion techniques [44]. In recent years many other techniques have been developed and used such as FTIR flow tubes [51], optical microscopy [52], electrodynamic balance experiments [53], continuous flow diffusion chambers [54], and large cloud expansion chambers [46].

3.2 Differential scanning calorimetry of emulsions

One experimental approach that has proven to be particularly successful for measuring the homogeneous freezing temperature of aqueous solutions is differential scanning calorimetry (DSC) of emulsified samples.

DSC is a very sensitive method to detect small amounts of heat that are released or absorbed by a sample. This makes DSC well suited to determine phase transitions in liquid or solid samples. DSC of emulsified samples can be considered the classic technique to study homogeneous ice nucleation in aqueous solutions. It was first introduced in the 1970s [44] and since has been widely applied in studies of supercooled water and aqueous solutions [17, 55]. Many properties of supercooled water have been obtained using emulsified water samples [1, 17, 56]. The reasoning behind the use of emulsified samples in DSC experiments is depicted in Fig. 6. A typical DSC sample size for determining a phase transition temperature in aqueous media is about 10^{-6} cm^3 (Fig. 6(a)). Such bulk samples are prone to heterogeneous nucleation due to ice nuclei usually contained in samples of such size. Supercooling to the




(a) Bulk		$V_{\text{tot}} \simeq 10^{-6} \text{ cm}^3$	Problem: heterogeneous ice nucleation
(b) Single Drop		$V_{\text{drop}} \simeq 10^{-11} \text{ cm}^3$	Problem: sensitivity too low
(c) Emulsion		$V_{\text{drop}} \simeq 10^{-11} \text{ cm}^3$ $V_{\text{tot}} \simeq 10^{-6} \text{ cm}^3$	Problems of (a) and (b) overcome

Fig. 6. Comparison between different methods of sample preparation in order to determine homogeneous ice nucleation in DSC experiments.

homogeneous ice nucleation temperature is usually achieved only in much smaller samples of about 10^{-11} cm^3 , such as a single drop $\sim 2.5 \mu\text{m}$ in diameter (Fig. 6(b)). Unfortunately, the latent heat released during the freezing of such a small droplet ($\sim 10^{-9} \text{ J}$) is far below the sensitivity of the best DSCs available ($\sim 10^{-7} \text{ J s}^{-1}$). Both, the ice nuclei as well as the sensitivity problems can be circumvented by preparing emulsion samples. The combined aqueous volume of all droplets (typically $\sim 10^{-6} \text{ cm}^3$) in the emulsion is large enough to warrant the detection of the latent heat released during freezing. At the same time, the dispersion into numerous small droplets in the micrometer size range ensures that ice nuclei are excluded from most of them. Therefore, supercooling to the homogenous nucleation temperature is usually achieved. An additional advantage of emulsion samples is the simultaneous probing of a large number of droplets ($\simeq 10^5$) in a single experiment.

Fig. 7 shows an experiment with an emulsified water sample. Upon cooling, ice nucleation occurs at about 235 K, a temperature considered to represent the homogeneous ice nucleation temperature for droplets of micrometer size [57]. The ice melting point is observed at 273 K, in agreement with the ice melting temperature of bulk samples. These observations indicate that the emulsification process affects the kinetics of the liquid-to-solid phase transition (by excluding ice nuclei), but not the thermodynamic properties of the aqueous samples. The same conclusions were reached when comparing ice melting points of emulsified and bulk aqueous solutions [58]. Other measurements have also confirmed the applicability of emulsified samples to determine fundamental thermodynamic properties of water in the supercooled state. For example, Archer and Carter [40] studied the isobaric heat capacity, c_p , of water in the supercooled state. They found very good agreement between c_p values obtained with emulsified and bulk samples.

One drawback of using emulsions is that the aqueous droplets usually exhibit a size distribution [59]. This is not of too much concern as long as only freezing temperatures are desired. However, in order to determine nucleation

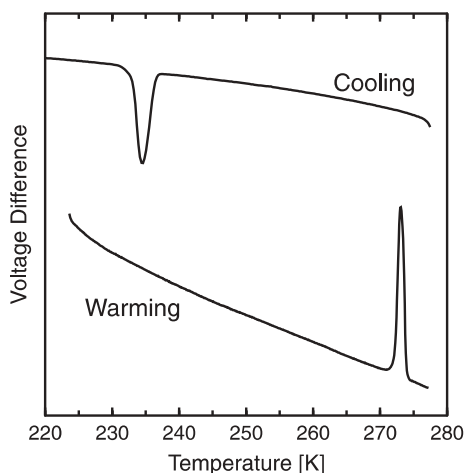


Fig. 7. DSC cooling and warming curves for emulsified water (data taken from [115]). The voltage difference is a measure of the latent heat that is released or absorbed during a phase transition in the sample. The curves are shifted vertically for clarity and the signal sizes are not to scale.

rate coefficients monodisperse droplets with a very narrow size distribution are required. Techniques to produce monodisperse emulsions do exist and have been used in freezing experiments [60, 61], but have never been applied to study nucleation rate coefficients.

3.3 Other techniques and open questions

Several other techniques have been developed and employed recently to study homogeneous ice nucleation in aqueous aerosol droplets [46, 51, 53, 54, 62–72]. It is interesting to note that the development of all these techniques was motivated by atmospheric ice formation processes.

Unfortunately, the homogeneous ice nucleation results from the various experimental techniques differ, in some cases substantially. This issue has been covered in detail in two recent articles [66, 67] and will be discussed here only briefly. It is important to point out that each technique defines the critical freezing temperature differently. One reason is that the various techniques possess a different sensitivity to the fraction of droplets that must be frozen in order to detect ‘freezing’. For example, microscope and emulsion techniques require the freezing of several 10% of the particles [52, 59] and continuous flow diffusion chamber experiments provide values for 0.1, 1, and 10% frozen particles [54]. FTIR flow tube techniques have a sensitivity that depends on experimental conditions (*e.g.*, temperature and aerosol droplet size) and which varies between 10^{-6} – 10^{-1} frozen particles [66]. The flow tube values are so variable because water mass transfer via gas phase diffusion from liquid to

frozen particles does occur during the residence time of the particles in the flow tube. This mass transfer can lead to a significant mass of ice detectable in the IR analysis, even when only 1 in 10^5 particles actually nucleated to form ice.

However, even when the different detection limits of the various techniques are taken into account significant differences between the different techniques remain [67]. The reason why the data of the different techniques cannot be reconciled is unclear. Further studies are needed in order to resolve these inconsistencies in the future.

4. Homogeneous ice nucleation in aqueous solutions

4.1 Freezing/melting point depression correlation

Solutes affect the equilibrium and non-equilibrium properties of water. The depression of the equilibrium ice melting point temperature is one such example. Similarly, the kinetic non-equilibrium process of ice nucleation is also affected by the presence of solutes. Data from a large number of solutions revealed that the supercooling required for homogeneous ice nucleation increases with increasing solute concentration [44, 73]. Based on these experimental data, Rasmussen suggested that the homogeneous freezing temperature depression, ΔT_f , and the equilibrium melting point depression, ΔT_m , are linearly correlated for aqueous solutions of a particular solute [73]:

$$\Delta T_f = \lambda \Delta T_m, \quad (1)$$

where $\Delta T_f = T_f^0 - T_f$ and $\Delta T_m = T_m^0 - T_m$. Here, $T_m^0 = 273.15 \text{ K}$ and $T_f^0 = 235 \text{ K}$ are the melting and the freezing temperatures of pure water, and T_m and T_f are, respectively, the experimentally determined melting and freezing temperatures of an aqueous solution. λ is independent of concentration and a constant that is specific for a particular solute. The formula by Rasmussen can be employed to correlate T_f with T_m when freezing data are available for a particular solute. It is in use for various applications [74, 75]. Once λ has been determined from fitting the data to Eq. (1), T_f for other concentrations of the same solute can be calculated. However, the formula lacks predictive capability for solutes where no T_f data are available, because it is not possible to deduce the value of λ from known properties of a solute without nucleation measurements.

4.2 Water-activity-based ice nucleation theory

The homogeneous freezing temperatures of aqueous solutions of various solutes show a large variability when plotted as a function of the total solute molality² (Fig. 8(a)). Likewise, the melting temperatures vary greatly. The

² The dissociation of strong electrolytes was taken into account, *i.e.*, the data for a 1 mol kg⁻¹ NaCl solution are shown at a concentration of 2 mol kg⁻¹ in Fig. 8(a).

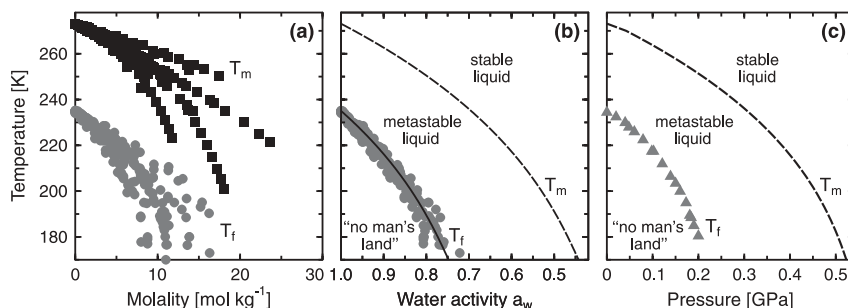


Fig. 8. Experimental melting and freezing data. **(a)** T_m (black squares) and T_f (grey circles) of micrometer-sized droplets as a function of total solute molality (salts and strong acids were treated as fully dissociated). Data of the following solutes were included: H_2SO_4 , HNO_3 , $\text{HNO}_3/\text{H}_2\text{SO}_4$, NH_4HSO_4 , $(\text{NH}_4)_2\text{SO}_4$, NH_4F , LiCl , NaCl , KCl , NH_4Cl , CaCl_2 , MnCl_2 , $\text{Ca}(\text{NO}_3)_2$, H_2O_2 , urea, ethylene glycol, glycerol, and glucose (for data sources see Ref. [78]), as well as MgCl_2 [116]. **(b)** the same data as in (a) as a function of the solution water activity, a_w . The dashed line is the melting point curve (a_w^i), the solid line is the melting point curve shifted by $\Delta a_w = 0.305$; **(c)** T_f and T_m for pure water droplets as a function of pressure [77, 117].

large variation in T_m and T_f of the various solutions reflects the non-ideal behavior of the solutions at moderate to high concentrations. To account for the non-ideality of the solutions, the same data are shown as a function of the solution water activity, a_w ,³ in Fig. 8(b). The melting point curves of the various solutions are now represented by a single line (dashed line in Fig. 8) because a_w of a solution in equilibrium with ice, a_w^i , is a function of temperature only, independently of the nature of the solute [76]. Also the freezing temperatures form a very compact distribution of data points, which is surprising given the large number of solutes contained in the data set. In addition, the T_f curve is observed to be horizontally parallel to the T_m curve. This is indicated by the solid line which was constructed by adding a constant offset Δa_w to the a_w^i curve (dashed) such that the solid line intersects the y-axis ($a_w = 1$) at 235 K, the homogeneous freezing temperature of micrometer-sized water droplets. The solid line describes the data points with a correlation coefficient of $r^2 = 0.96$ providing strong evidence that the kinetic (non-equilibrium) ice nucleation process is entirely driven by thermodynamic (equilibrium) quantities.

In Fig. 8(c) the T_m and T_f curves are shown for pure water as a function of pressure [77]. The very similar shape of the curves when compared to those in Fig. 8(b) suggests that solutes or applied pressure have a very similar effect on T_m and T_f . However, the apparent similarities between the two curves do not allow the conclusion that the driving force for ice nucleation is indeed the same in both cases. Because the data in Fig. 8(b) suggest a thermodynamic

³ The water activity of a solution is equal to the ratio between the water vapor pressures of the solution and of pure water under the same conditions.

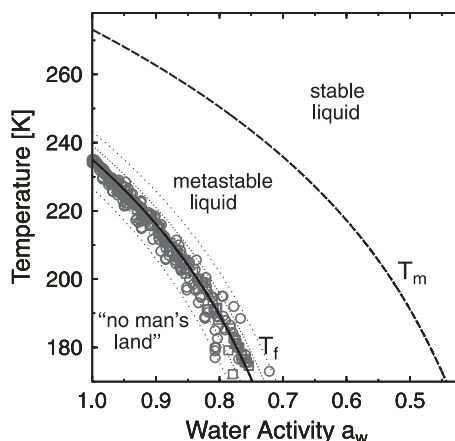


Fig. 9. All data from aqueous solutions at ambient pressure (circles), pure water subject to mechanical pressure (triangles), and aqueous solutions subject to mechanical pressure (squares) evaluated according to Eq. (2). The data shown as circles and triangles have been taken from Fig. 8, the data shown as squares are from Ref. [118]. The black line is the same as in Fig. 8(b). The light and heavy dotted lines indicate a deviation in a_w of 2.5% and 5%, respectively, around the black line.

driving force for homogeneous ice nucleation in aqueous solutions, it was investigated whether the data in Fig. 8(b) and Fig. 8(c) could be merged into a single curve based on thermodynamic principles [78]. Therefore, the concentration, temperature, and pressure dependent water chemical potentials of aqueous solutions, $\mu_w(c, T, p)$, and of pure ice, $\mu_w^i(T, p)$, were studied and it was proposed that a solution with concentration c under pressure p freezes at the same temperature as another solution with concentration c_{eff} under zero pressure⁴ when the differences between the chemical potentials of water in the solution and in ice are the same [78]:

$$\mu_w(c, T, p) - \mu_w^i(T, p) = \mu_w(c_{\text{eff}}, T, 0) - \mu_w^i(T, 0). \quad (2)$$

All freezing data were analyzed and transferred to zero pressure according to Eq. (2). The results of this analysis are shown in Fig. 9, which contains data from aqueous solutions at ambient pressure (Fig. 8(b)), from pure water subject to mechanical pressure (Fig. 8(c)), and from aqueous solutions subject to mechanical pressure (not shown separately). Fig. 9 clearly reveals that homogeneous ice nucleation is indeed driven entirely by thermodynamic parameters.

At this point a discussion is in order about the physical background for the observed thermodynamic control of ice nucleation. It has been discussed above

⁴ An ambient pressure of 10^{-4} GPa is negligible on the scale of Fig. 8(c) and can be treated as zero.

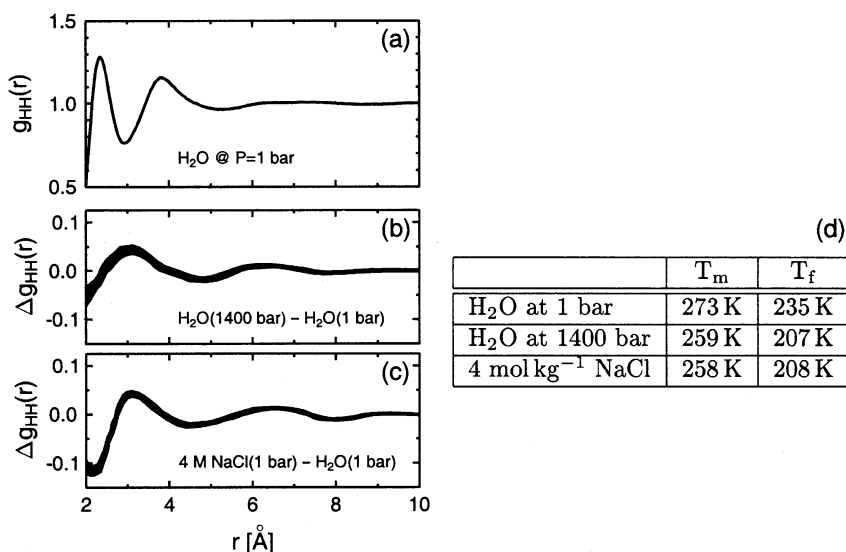


Fig. 10. Hydrogen–hydrogen (HH) radial distribution functions from neutron diffraction experiments. **(a)** for water at ambient pressure and a temperature of 298 K [79]; **(b)** changes in the HH radial distribution functions between the curve shown in (a) and water at a pressure of 1400 bar [82]; **(c)** changes between the curve shown in (a) and a 4 mol kg⁻¹ NaCl solution [82]. **(d)** Experimental T_m and T_f values for the three cases shown in (a)–(c).

that the peculiar properties of supercooled water arise from the interactions between water molecules via hydrogen bonds. The preferred local structure is a tetrahedral coordination. This is a consequence of the nearly tetrahedral arrangement of the two hydrogen atoms and the two free electron pairs around the central oxygen atom in a water molecule. Neutron diffraction experiments can provide information on the structural arrangement of water molecules in the condensed phase. The hydrogen–hydrogen (HH) radial distribution function for water at 298 K and ambient pressure is shown in Fig. 10(a) [79]. This correlation function provides information on intermolecular distances of hydrogen atoms in neighboring water molecules. The two pronounced positive peaks at 2.4 Å and 3.8 Å are caused by strong orientational correlations between neighboring water molecules in hydrogen bonded water. The peak at 2.4 Å corresponds to the HH separation (across an intervening oxygen) in a H···OH hydrogen bond, while the peak at 3.8 Å corresponds to the HH distance between pairs of molecules that are not hydrogen bonded [80, 81].

The water structure and, hence, the correlation functions change when mechanical pressure is applied or solutes are added. The associated changes in the correlation functions for two such cases are shown in Fig. 10(b) and (c): one for the application of a pressure of 1400 bar (= 0.14 GPa), and the other for the addition of 4 moles of NaCl per kg of water. In both cases the 2.4 Å

and 3.8 Å peaks are diminished implying that the orientational correlations are weakened [82]. Based on the similarities between the changes in Fig. 10(b) and (c) and on comparisons to other data, Leberman and Soper concluded that the addition of 4 mole NaCl per kg of water has an equivalent effect on the water structure as increasing the pressure applied to pure water to 0.14 GPa [82]. In Fig. 10(d), the corresponding melting and freezing temperatures are shown for the conditions of Fig. 10(a)–(c). We find $T_m = 259$ K and $T_f = 207$ K for pure water at 0.14 GPa, and $T_m = 258$ K and $T_f = 208$ K for a 4 molal NaCl solution. The very good agreement between these values suggests that the T_m and T_f values are a consequence of the very similar hydrogen bonding of water in the two cases.

But how can the state of water's hydrogen bonding network be responsible for the locus of the T_f line? This question brings us back to the discussion on the theories of liquid water in the supercooled range. All of these theories attribute the observed changes in the properties of water with pressure and temperature to changes in the hydrogen bonds between water molecules. Since the neutron diffraction experiments suggest that solutes induce a change in water structure that is equivalent to the application of pressure, it appears natural to discuss the implications that the theories for water might have for a possible explanation of ice nucleation in aqueous solutions.

According to the stability limit theory a spinodal temperature, T_s , exists below which the liquid phase becomes unstable. Such a spinodal has been proposed to exist also in aqueous solutions [83]. Ice nucleation is suggested not to occur at the spinodal temperature itself, but at T_f a few kelvins above T_s . A physical picture of ice nucleation in aqueous solutions based on the spinodal scenario has been suggested by Rasmussen and coworkers [83, 84]. As the liquid phase approaches the spinodal, order and/or concentration fluctuations in the liquid become larger allowing the local demixing of the liquid parent phase into two daughter phases. This triggers the formation of an ice germ that is in local equilibrium with one of the daughter phases. After the fluctuation is over, the germ can grow if it is supersaturated within the liquid parent phase. Since the locus of any spinodal is determined exclusively by external thermodynamic properties, this approach suggests that the kinetic ice nucleation process can be described entirely through thermodynamic parameters [83, 84], in agreement with the conclusions drawn above.

The other two theories of supercooled water might also be suitable for providing a physical explanation for the observed ice nucleation behavior in aqueous solutions. For example, a singularity-free scenario for aqueous solutions might predict order fluctuations to increase strongly around T_f , thereby increasing the likelihood for the formation of a critical germ and, hence, homogeneous ice nucleation. Studies on aqueous NaCl solutions lend support to the singularity-free scenario in supercooled aqueous solutions [40]. Similarly, a possible existence of a second critical point in water or even aqueous solutions might have comparable effects on ice nucleation. This is supported by

a recent model simulation which suggests that the location of T_i corresponds to the calculated position of extrema in the isothermal compressibility of water, κ [85]. It is argued that at higher values of κ , density fluctuations in the liquid are larger and, thus, also the chance for the occurrence of regions where the density of water approaches that of ice. As a consequence, ice germs can form more easily in these regions and the nucleation rate is increased.

It is difficult to prove which of the theories of liquid water, if any, is correct. The result will also have implications for our understanding of aqueous solutions at low temperature and might pave the way for more detailed molecular dynamics simulations of ice nucleation [86] in supercooled solutions. At the moment, it appears that more theoretical and experimental studies are needed in order to solve one of the great open puzzles in research on water.

4.3 Water activity of supercooled aqueous solutions

The application of water-activity-based ice nucleation theory requires knowledge of a_w for aqueous solutions in the supercooled region. However, direct measurements of a_w for aqueous solutions supercooled with respect to ice are not available. Thermodynamic models for inorganic solutions exist that provide a_w values for a large range of concentrations down to ~ 180 K [87]. The temperature range of the model predictions reach well into the supercooled range and also into the “no man’s land” of aqueous solutions (see Fig. 4). Clearly, these predictions are based on extrapolations whose accuracy in the supercooled range remain uncertain. In addition, these models usually apply to a limited number of inorganic solutes only [88]. For aqueous solutions of other solutes an extrapolation of a_w to low temperatures is required from data in the accessible region. Most of the data in Fig. 8 have been derived under the assumption that a_w is independent of temperature for solutions of fixed composition. This is a reasonably good assumption in many cases, as can be shown by investigating the temperature dependence of a_w at temperatures above T_m . The differences are usually smaller than a few percent [76, 87, 89]. The light and heavy dotted lines in Fig. 9 indicate a deviation of 2.5% and 5%, respectively, from the predicted freezing line. All data are within the 5% area and most of the data at higher temperature even within the 2.5% area. This indicates that the observed spread of the data around the model prediction can easily be due to uncertainties in estimating a_w of the solutions at low temperatures.

There are, however, notable exceptions. The most important ones are probably solutions of Poly[ethylene glycol], PEG, which show strong dependencies of a_w with temperature [90]. Another case, although less pronounced, appears to be ammonium nitrate, NH_4NO_3 [91]. Fig. 11 shows a_w for several solutions of PEG oligomers with an average molar mass of 300 g mol^{-1} (PEG300), H_2SO_4 , and NH_4NO_3 . While a_w of the different H_2SO_4 solutions is nearly independent of temperature, a_w decreases with decreasing temperature in the PEG300 solutions. This behavior is in agreement with results of a physical

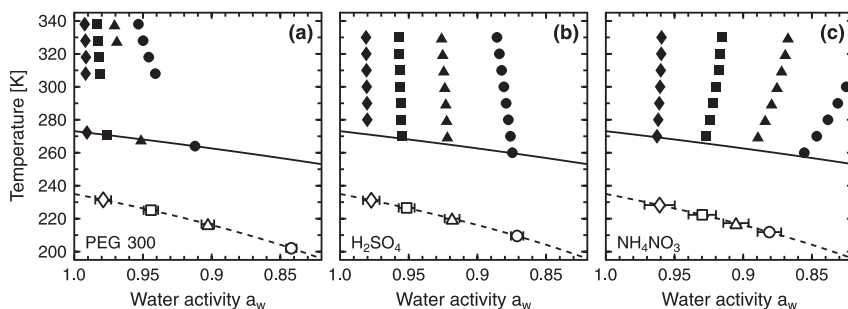


Fig. 11. The water activity, a_w , of various aqueous solutions of PEG300 (a), H_2SO_4 (b) and NH_4NO_3 (c) at different temperatures. Solid symbols are water activities derived from experimental data [90] or thermodynamic models [87]. The solid line represents the ice melting point curve. The dashed line and open symbols are water activities predicted by water-activity-based ice nucleation theory. Concentrations for PEG300 are 10.8, 20.0, 29.9, and 39.3 wt%, for H_2SO_4 5, 10, 15, and 20 wt%, and for NH_4NO_3 10, 20, 30, and 40 wt%. The T_f values for PEG300 have been taken from Ref. [90], for H_2SO_4 from Ref. [52], and for NH_4NO_3 from Ref. [91].

model of aqueous PEG solutions that includes competitive hydrogen bonding between water–water and water–polymer molecules [92]. The model does predict a very strong change in water activity of PEG solutions in the supercooled temperature range, just as observed. Qualitatively, this behavior can be understood as follows. PEG molecules are dissolved in water through the formation of water–PEG hydrogen bonds. At low temperatures an increasing number of PEG molecules are hydrogen bonded to water, leading to a reduction of the solution water activity [93].

In contrast, a_w in the NH_4NO_3 solutions increases with decreasing temperature, suggesting a decreasing interaction between the solute and water upon cooling. One possible explanation might be an increasing association of $\text{NH}_4^+(\text{aq})$ and $\text{NO}_3^-(\text{aq})$ ions with decreasing temperature, thereby forming $\text{NH}_4\text{NO}_3(\text{aq})$ ion-pairs in the solution. This seems not unreasonable because measurements and model predictions show that the solubility of NH_4NO_3 decreases very strongly upon cooling [87].

Solutions that exhibit strong changes in a_w with temperature can be used to test water-activity-based ice nucleation theory. Fig. 11 also includes measured ice freezing temperatures of PEG300, H_2SO_4 , and NH_4NO_3 solutions as open symbols. Since the water activities of the solutions at T_f were not measured, water-activity-based ice nucleation theory was used to predict them, *i.e.*, $a_w(T_f)$ was chosen to be in perfect agreement with the model (dashed line). These predicted water activities in the supercooled region can now be compared to measured water activities at temperatures above T_m . Fig. 11 indicates that the predicted a_w values are consistent with the measured a_w values, thus indirectly supporting water-activity-based ice nucleation theory.

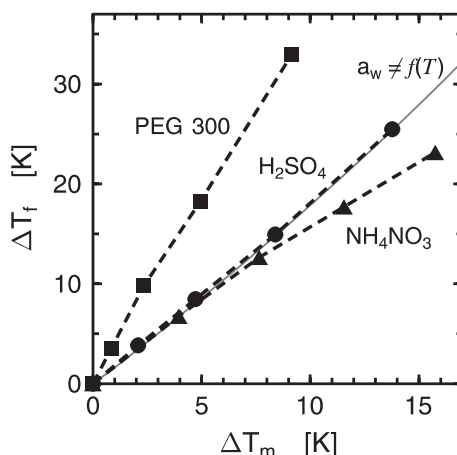


Fig. 12. The freezing temperature depression, ΔT_f , as a function of the equilibrium melting point depression, ΔT_m , for the data shown in Fig. 11. The thin grey line indicates the behavior of a hypothetical solute whose aqueous solutions do not exhibit any temperature dependence of a_w .

It appears from Fig. 11 that solutions of PEG300 show a larger supercooling ability than those of H_2SO_4 , and that the supercooling of NH_4NO_3 solutions is even lower. This fact is more clearly revealed in Fig. 12 in which the measured T_m and T_f values were used to calculate ΔT_f as a function of ΔT_m for the different solutes. Also shown as the thin grey line is ΔT_f as a function of ΔT_m for a hypothetical solute whose aqueous solutions do not exhibit any temperature dependence of a_w . (This would correspond to perfectly vertical lines at all concentrations in Fig. 11.) As can be seen, H_2SO_4 solutions come very close to this behavior. In contrast, the decreasing a_w in aqueous PEG solutions in Fig. 11(a) leads to enhanced ΔT_f values in Fig. 12. The behavior of NH_4NO_3 is just the opposite: increasing a_w in solutions upon cooling (Fig. 11(c)) leads to reduced ΔT_f values. The comparison in Fig. 12 suggests that the different λ values in this type of plot are a direct result of the temperature dependence of a_w in aqueous solutions of a given solute. To corroborate this proposal a sensitivity study has been performed. A very simple model has been chosen to describe the temperature and concentration dependence of a_w in hypothetical solutions. It is assumed that a_w changes linearly with temperature below T_m as

$$a_w(T) = a_w(T_m) + m[T_m - T]. \quad (3)$$

The magnitude of this temperature dependence, m , is chosen to become stronger with decreasing a_w (*i.e.*, increasing solute concentration):

$$m = m^0[1 - a_w^i]. \quad (4)$$

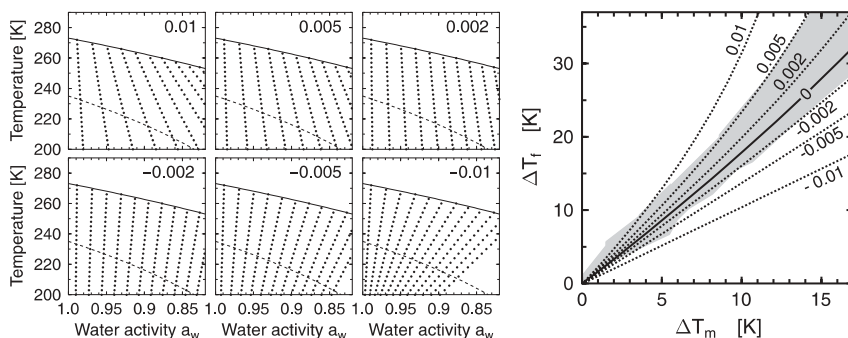


Fig. 13. The effect of temperature dependent a_w values on ΔT_f versus ΔT_m correlations. The left panel shows a_w values for solutions of six hypothetical solutes at different concentrations. The number in the top right corner of each plot indicates the value of m^0 used to calculate a_w according to Eq. (3). The right panel shows the corresponding ΔT_f versus ΔT_m correlations. The black line corresponds to $m^0 = 0$.

The resulting temperature dependence of a_w is shown in the left panel of Fig. 13 for six cases with m^0 varying from -0.01 to $+0.01$. The right panel of Fig. 13 depicts the corresponding ΔT_f versus ΔT_m correlations. The larger m^0 , the greater is the slope of the ΔT_f versus ΔT_m correlations. Note that a linear relationship between ΔT_f and ΔT_m is not mandatory. Depending on the actual a_w behavior, non-linear relations may result, and the data of NH_4NO_3 solutions in Fig. 12 do indeed show a non-linear relationship. The grey area in Fig. 13 indicates the range of data for all solutes shown in Fig. 9. The data correspond to a_w changes with m^0 values between 0.005 and -0.002 . Such small changes are conceivable. This comparison suggests that the observed spread of the data in Fig. 9 is very likely due to the fact that all these solutions exhibit small temperature dependencies of a_w , which were not taken into account in the analysis.

5. Ice nucleation rate coefficients

5.1 Volume dependent nucleation

Up to now, we have treated the homogeneous ice nucleation temperature, T_i , as if it was a fixed temperature. However, this is a simplification because ice nucleation is a stochastic process. In the following we will treat the kinetics of the ice nucleation process more explicitly. Let us consider a sample that consists of m water molecules each of which has a probability p to become the center of a critical germ during a certain observation time. For large m and $p \ll 1$ (i.e., a very small molecular nucleation probability) we can define the nucleation rate

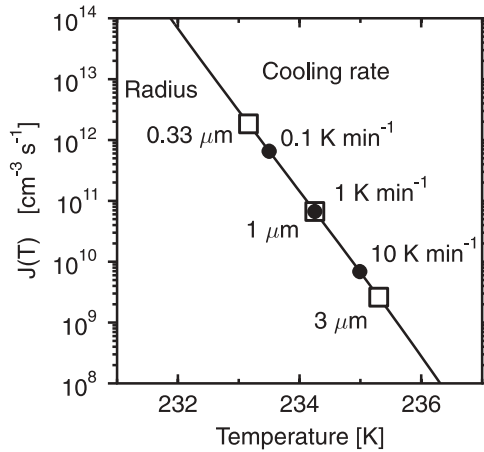


Fig. 14. The homogeneous volume nucleation rate coefficient of ice in water, $J(T)$, as a function of temperature (black line [95]). The data points indicate the median freezing temperatures of water droplets for various conditions; squares: for droplets of different size at a cooling rate of 1 K min^{-1} , circles: for different cooling rates and a droplet with a radius of $1 \mu\text{m}$.

ω (in s^{-1}) of the whole sample

$$\omega \equiv m p/t, \quad (5)$$

where t is time (in s), and p/t is the nucleation rate for a single molecule in the sample [94]. Therefore, the probability that a sample is frozen after time t (because a nucleation event has occurred) is

$$P_f(t) = 1 - \exp(-\omega t). \quad (6)$$

The freezing rate ω of a water sample depends on parameters such as temperature and sample size. Since the chance for the formation of a stable ice germ is proportional to number of molecules that can become the center of such a germ, ω can be written as the product $\omega = J(T)V$, where V is the sample volume (in cm^3) and $J(T)$ is the temperature dependent homogeneous volume nucleation rate coefficient of ice in water (in $\text{cm}^{-3} \text{s}^{-1}$). Based on a large number of ice nucleation measurements with variable sample sizes Prupacher has provided a parameterization of $J(T)$ for pure water which is shown in Fig. 14 [95].

$J(T)$ exhibits a strong temperature dependence: it changes by 6 orders of magnitude in a temperature interval of about 4 K. We can use this formulation of $J(T)$ to calculate the median freezing temperature, T_f^{50} , for samples that are

cooled at a certain cooling rate by numerically integrating⁵

$$\int_{T_m}^{T_i^{50}} J(T') dT' = \frac{\gamma \ln(0.5)}{V}, \quad (7)$$

where T_m is the melting temperature and $\gamma = -dT/dt$ is the cooling rate. The results for selected droplet sizes and cooling rates are also shown in Fig. 14. They indicate that moderate variations in cooling rate or sample volume have only a minor effect on the observed median freezing temperature. For example, increasing the cooling rate by a factor of 100 leads to a reduction in T_i^{50} of less than 2 K. This insensitivity of T_i^{50} to changes in cooling rate or sample volume is the reason why using a ‘fixed’ T_i value was justified in the discussion above.

However, in many applications such as atmospheric ice cloud particle formation, changes in droplet size and cooling rate are a more critical issue. In order to apply the above to homogeneous ice nucleation in aqueous solutions the effect of solutes on $J(T)$ have to be considered, and parameterizations for J as a function of temperature and water activity do exist [78].

5.2 Surface dependent nucleation

Recently, Tabazadeh and coworkers have proposed that liquid-to-solid nucleation in droplets surrounded by a gas occurs preferentially at the surface of the droplets and not in their interior [96–98]. This suggestion implies that nucleation rates are proportional to droplet surface area rather than to droplet volume as is usually assumed [57]. Below, we will discuss the implications of this suggestion for ice nucleation in water droplets.

Tabazadeh and coworkers have used the framework of classical nucleation theory [98]. In this theory the formation of a critical germ is largely affected by the surface energy between the solid germ and the surrounding liquid, σ_{ls} . The smaller this surface energy σ_{ls} , the more likely nucleation is to occur. In order to treat liquid-to-solid nucleation at the gas/liquid interface, the gas/liquid surface energy, σ_{gl} , and the gas/solid surface energy, σ_{gs} , were also considered. Based on thermodynamic arguments they derived a necessary condition for surface nucleation [96]

$$\sigma_{gs} - \sigma_{gl} < \sigma_{ls}. \quad (8)$$

If this condition is fulfilled, the probability for a water molecule at the droplet surface to become the center of a critical ice germ, p_s , is larger than that of a molecule in the interior of the droplet, p_v . Based on Eq. (5) we can define the surface nucleation rate, $\omega_s \equiv m_s p_s / t$, and the corresponding volume nucleation

⁵ T_i^{50} is defined as the temperature at which 50% of the samples are frozen.

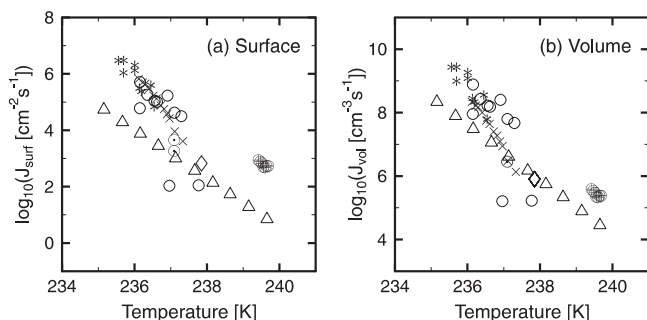


Fig. 15. Ice nucleation data for liquid water droplets in gaseous environments. The data have been evaluated assuming nucleation occurred (a) on the surface or (b) in the volume of the droplets. Triangles, $r = 2.5 \mu\text{m}$ [45]; circles, $r = 20 \mu\text{m}$, and asterisks, $r = 33 \mu\text{m}$ [50]; diamonds, $r = 12-45 \mu\text{m}$ [101]; circles with plus sign, $r = 20-22.5 \mu\text{m}$ [99]; crosses, $r = 30 \mu\text{m}$ [48]; and circles with dots, $r = 19-49 \mu\text{m}$ [100].

rate, $\omega_v \equiv m_v p_v / t$, for a sample. Comparing ω_s with ω_v shows that fulfillment of Eq. (8) is not sufficient to conclude that $\omega_s > \omega_v$ because m_v is much larger than m_s unless the droplets are extremely small ($< 1 \text{ nm}$ in the case of water). Unfortunately, the different surface energies are not available at temperatures in the supercooled regime so that ω_s and ω_v cannot be calculated. Measurements are needed in order to conclude whether surface nucleation or volume nucleation is the dominant process.

Tabazadeh *et al.* evaluated a number of different emulsion experiments [98]. They showed that some data sets were consistent with a volume dependent process while other data sets were more consistent with a surface dependent process. This led them to the conclusion that in some emulsion experiments the presence of surfactants at the oil/water interface prevents surface nucleation. In these cases volume nucleation is the favored nucleation process. They further proposed that for droplets in air surface nucleation is the preferred nucleation process. Two data sets for water droplets in air were included in the analysis, one from expansion chamber experiments [45] and another from electrodynamic balance experiments [48, 99]. Since the two data sets did not agree within experimental uncertainties when evaluated in terms of surface nucleation, only data from droplets with a radius of $2.5 \mu\text{m}$ was used for parameterizing surface nucleation rate coefficients. However, no experimental evidence was presented that the ice nucleation process in water drops surrounded by air does indeed occur at the surface.

Fig. 15 provides a more comprehensive overview of data on ice nucleation in water droplets in gaseous environments. Several data sets, available in the literature, have been used [45, 48, 50, 99–101]. The ice nucleation data of the different experiments have been evaluated by assuming nucleation to occur (a) at the surface or (b) in the volume. The resulting nucleation rate coefficients are depicted in Fig. 15. Unfortunately, the comparison in Fig. 15 is inconclu-

sive because the scatter in the data is too large. It is similar in magnitude in both plots, indicating that neither surface dependent nucleation nor volume dependent nucleation are convincingly supported by this analysis. It appears that the differences between the small droplet data and larger droplet data are somewhat smaller in the volume nucleation plot (Fig. 15(b)) when compared to the surface nucleation plot (Fig. 15(a)). However, given the magnitude of the scatter this cannot be regarded as conclusive evidence.

It should be mentioned that the emulsion and droplets in air studies discussed in Ref. [98] are all consistent with an alternative interpretation using the classic volume nucleation based picture: Ice nucleation normally occurs in the interior of droplets, *i.e.*, is a volume dependent process. This is valid for drops in air and for some of the emulsion experiments. However, in other emulsion experiments heterogeneous ice nucleation is initiated at the water/surfactant interface. It is well known that certain surfactants arranged in monolayers at the surface of water drops are efficient ice nucleating agents [102]. Hence all experimental observations can equally well be explained by assuming homogeneous ice nucleation in droplets surrounded by air being a volume dependent process.

In conclusion, the proposal of surface nucleation is certainly a very intriguing idea. Whether or not surface nucleation occurs in droplets surrounded by air is an important question that should definitely be pursued further by suitable experiments. However, at present there is no conclusive evidence that homogeneous ice nucleation in water or aqueous solutions does indeed occur by this process.

6. Conclusions and outlook

There is ample evidence suggesting that the kinetic homogeneous ice nucleation process in water and aqueous solutions is entirely determined by thermodynamic equilibrium properties. This can be shown from an analysis of experimental data from a wide range of solutes, both at ambient pressure and under large mechanical pressures. Plausible physical reasons for the observed behavior have been discussed in the light of three currently proposed theories for supercooled liquid water.

Freezing rate measurements in pure water droplets surrounded by a gas have been analyzed with respect to the recent proposal that ice nucleation occurs at the droplet surface in such cases. However, neither a surface dependent nucleation process nor a volume dependent nucleation process are supported, the analysis remains inconclusive because the scatter in the experimental data of the various techniques is too large.

The results and concepts presented in this review raise a number of questions and topics that should be investigated in the future. A few of them are presented below.

Theories of water One of the biggest open questions in research on water is a more detailed understanding of the origin of the unusual properties of water, particularly in the supercooled temperature range. Additional efforts in theoretical approaches and new experimental studies will be needed in order to answer which of the three theories for liquid water, if any, is correct. At the same time, the implications of these theories for our understanding of aqueous solutions at low temperatures are largely unexplored since most studies have been devoted to pure water so far. Therefore, aqueous solutions provide an open 'playground' for similar investigations in the future.

Disagreement between experimental techniques A more technical, but not unimportant topic is the apparent discrepancy between homogeneous ice nucleation results from different experimental techniques. We need to understand whether these differences are real, *i.e.*, are a consequence of the different experimental sensitivities to the magnitude of the nucleation rate, or whether they are due to experimental artifacts.

Surface based nucleation One important question is whether homogeneous ice nucleation in water or aqueous solution droplets in a gaseous environment does occur at the droplet surface or not. At present, an answer to this question can only come from laboratory experiments. Two approaches appear to be possible. Firstly, detecting the location of freshly nucleated ice germs at the nanometer scale, or secondly, designing experiments that cover a wide range of droplet sizes in order to determine whether the nucleation kinetics obeys a quadratic or cubic radius dependence.

Biological applications It is believed that ice nucleation in the interior of cells is lethal to organisms in most cases [103]. A substantial portion of the ecosphere is subject to subfreezing temperatures either permanently or seasonally. It is known, that plants and insects produce polyols to prepare themselves for wintertime temperatures [103, 104]. In the laboratory, PEG solutions have been shown to be a suitable medium for the storage of living cells at low temperatures [105]. A first step to understand this suitability of PEG solutions to enable large supercooling has been to show their strong a_w temperature dependence [90]. One way to proceed in this area could be to design specific solutions that exhibit an even larger temperature dependence of a_w : at room temperature high a_w values close to 1 are desired to provide isotonic conditions, at low temperatures small a_w values are preferred to avoid lethal ice nucleation in the cells.

Homogeneous versus heterogeneous nucleation No satisfactory theoretical framework for the description of heterogeneous ice nucleation is currently available. First attempts have been made to use water-activity-based ice nucleation theory for parameterizing heterogeneous immersion freezing in aqueous

droplets for atmospheric purposes [106]. It will be important to investigate experimentally and theoretically how the properties of both, ice nuclei and dissolved solutes, affect the nucleation of ice in aqueous systems. Such studies will also have implications for cryobiological applications, since it has been argued that ice nucleation in biological systems is predominantly heterogeneous [107].

The diversity of the topics raised above indicates that fundamental studies and applied research must go hand in hand in order to solve these open questions. It also stresses the importance of interdisciplinary work in this area of research.

Acknowledgement

Many colleagues have contributed, directly or indirectly, to this work; in particular I would like to thank Marcia Baker, Allan Bertram, Daniel Knopf, Beiping Luo, Mario Molina, Thomas Peter, Uwe Weers, and Beni Zobrist for their support.

References

1. O. Mishima and H. E. Stanley, *Nature* **396** (1998) 329.
2. W. E. K. Middleton, *The experimenters – A study of the accademia del cimento*, The John Hopkins Press, Baltimore (1971).
3. D. W. Oxtoby, Nucleation and surface melting of ice, in *Ice Physics and the Natural Environment*, J. S. Wettlaufer, J. G. Dash, N. Untersteiner (Eds.), vol. I 56, pp. 23–38, Berlin (1999), NATO ASI Series, Springer.
4. D. G. Fahrenheit, *Philos. Trans. R. Soc. London* **33** (1724) 78 (german translation in: Ostwald's Klassiker der exakten Wissenschaften, 57, *Abhandlungen über Thermometrie von Fahrenheit, Réaumur, Celsius (1724, 1730–1733, 1742)*, A. J. von Oettigen (Ed.), Engelmann, Leipzig (1894)).
5. C. T. R. Wilson, *Philos. Trans. R. Soc. London A* **189** (1897) 265.
6. B. M. Cwilong, *Proc. R. Soc. Lond. A* **190** (1947) 137.
7. V. J. Schaefer, *Science* **104** (1946) 457.
8. V. J. Schaefer, *Bull. Am. Meteorol. Soc.* **29** (1948) 175.
9. P. Brüggeller and E. Mayer, *Nature* **288** (1980) 569.
10. V. Velikov, S. Borick, and C. A. Angell, *Science* **294** (2001) 2335.
11. Y. Z. Yue and C. A. Angell, *Nature* **427** (2004) 717.
12. O. Mishima, L. D. Calvert, and E. Whalley, *Nature* **314** (1985) 76.
13. P. G. Debenedetti, *J. Phys. Condens. Matter* **15** (2003) R1669.
14. P. G. Debenedetti, *Metastable liquids*, Princeton University Press, Princeton, NJ (1996).
15. R. J. Speedy and C. A. Angell, *J. Chem. Phys.* **65** (1976) 851.
16. R. J. Speedy, *J. Phys. Chem.* **86** (1982) 982.
17. C. A. Angell, Supercooled water, in *Water a comprehensive treatise*, F. Franks (Ed.), vol. 7, pp. 1–81, Plenum Press, New York (1982).
18. S. Sastry, P. G. Debenedetti, F. Sciortino, and H. E. Stanley, *Phys. Rev. E* **53** (1996) 6144.

19. L. P. N. Rebelo, P. G. Debenedetti, and S. Sastry, *J. Chem. Phys.* **109** (1998) 626.
20. P. H. Poole, F. Sciortino, U. Essmann, and H. E. Stanley, *Nature* **360** (1992) 324.
21. P. H. Poole, F. Sciortino, T. Grande, H. E. Stanley, and C. A. Angell, *Phys. Rev. Lett.* **73** (1994) 1632.
22. O. Mishima and Y. Suzuki, *Nature* **419** (2002) 599.
23. O. Mishima and H. E. Stanley, *Nature* **392** (1998) 164.
24. O. Mishima, *Phys. Rev. Lett.* **85** (2000) 334.
25. T. Loerting, C. Salzmann, I. Kohl, E. Mayer, and A. Hallbrucker, *Phys. Chem. Chem. Phys.* **3** (2001) 5355.
26. J. L. Finney, D. T. Bowron, A. K. Soper, T. Loerting, E. Mayer, and A. Hallbrucker, *Phys. Rev. Lett.* **89** (2002) 205503.
27. C. A. Tulk, C. J. Benmore, J. Urquidi, D. D. Klug, J. Neuefeind, B. Tomberli, and P. A. Egelstaff, *Science* **297** (2002) 1320.
28. D. D. Klug, *Nature* **420** (2002) 749.
29. I. Brovchenko, A. Geiger, and A. Oleinikova, *J. Chem. Phys.* **118** (2003) 9473.
30. M. C. Bellissent-Funel, L. Bosio, A. Hallbrucker, E. Mayer, and R. Sridi-Dorbez, *J. Chem. Phys.* **97** (1992) 1282.
31. M. C. Bellissent-Funel and L. Bosio, *J. Chem. Phys.* **102** (1995) 3727.
32. L. S. Bartell and J. Huang, *J. Phys. Chem.* **98** (1994) 7455.
33. J. Huang and L. S. Bartell, *J. Phys. Chem.* **99** (1995) 3924.
34. C. H. Heath, K. Streletzky, B. E. Wyslouzil, J. Wölk, and R. Strey, *J. Chem. Phys.* **117** (2002) 6176.
35. A. Khan, C. H. Heath, U. M. Dieregswiler, B. E. Wyslouzil, and R. Strey, *J. Chem. Phys.* **119** (2003) 3138.
36. Y. J. Kim, B. E. Wyslouzil, G. Wilemski, J. Wölk, and R. Strey, *J. Phys. Chem. A* **108** (2004) 4365.
37. C. E. L. Myhre, D. H. Christensen, F. M. Nicolaisen, and C. J. Nielsen, *J. Phys. Chem. A* **107** (2003) 1979.
38. D. A. Knopf, B. P. Luo, U. K. Krieger, and T. Koop, *J. Phys. Chem. A* **107** (2003) 4322.
39. K. Tomikawa and H. Kanno, *J. Phys. Chem. A* **102** (1998) 6082.
40. D. R. Archer and R. W. Carter, *J. Phys. Chem. B* **104** (2000) 8563.
41. B. Vonnegut, *J. Colloid Sci.* **3** (1948) 563.
42. P. G. Fox, *Nature* **184** (1959) 546.
43. G. R. Wood and A. G. Walton, *J. Appl. Phys.* **41** (1970) 3027.
44. D. H. Rasmussen and A. P. MacKenzie, Effect of solute on ice-solution interfacial free energy; calculation from measured homogeneous nucleation temperatures, in *Water structure at the water polymer interface*, H. H. G. Jellinek (Ed.), pp. 126–145, Plenum Press, New York (1972).
45. P. J. DeMott and D. C. Rogers, *J. Atmos. Sci.* **47** (1990) 1056.
46. O. Möhler, O. Stetzer, S. Schaefers, C. Linke, M. Schnaiter, R. Tiede, H. Saathoff, M. Krämer, A. Mangold, P. Budz, P. Zink, J. Schreiner, K. Mauersberger, W. Haag, B. Kärcher, and U. Schurath, *Atmos. Chem. Phys.* **3** (2003) 211.
47. B. Krämer, M. Schwell, O. Hübner, H. Vortisch, T. Leisner, E. Rühl, H. Baumgärtel, and L. Wöste, *Ber. Bunsenges. Phys. Chem.* **100** (1996) 1911.
48. B. Krämer, O. Hübner, H. Vortisch, L. Wöste, T. Leisner, M. Schwell, E. Rühl, and H. Baumgärtel, *J. Chem. Phys.* **111** (1999) 6521.
49. D. Salcedo, L. T. Molina, and M. J. Molina, *Geophys. Res. Lett.* **27** (2000) 193.
50. S. E. Wood, M. B. Baker, and B. D. Swanson, *Rev. Sci. Instr.* **73** (2002) 3988.
51. A. K. Bertram, D. D. Patterson, and J. J. Sloan, *J. Phys. Chem.* **100** (1996) 2376.
52. T. Koop, H. P. Ng, L. T. Molina, and M. J. Molina, *J. Phys. Chem. A* **102** (1998) 8924.

53. H. Vortisch, B. Krämer, I. Weidinger, L. Wöste, T. Leisner, M. Schwell, H. Baumgärtel, and E. Rühl, *Phys. Chem. Chem. Phys.* **2** (2000) 1407.
54. Y. Chen, P. J. DeMott, S. M. Kreidenweis, D. C. Rogers, and D. E. Sherman, *J. Atmos. Sci.* **57** (2000) 3752.
55. F. Franks, The properties of aqueous solutions at subzero temperatures, in *Water a comprehensive treatise*, F. Franks (Ed.), vol. 7, pp. 215–338, Plenum Press, New York (1982).
56. C. A. Angell, *Ann. Rev. Phys. Chem.* **34** (1983) 593.
57. H. R. Pruppacher and J. D. Klett, *Microphysics of clouds and precipitation*, Kluwer, Dordrecht (1997) 2nd edition.
58. T. Koop, A. K. Bertram, L. T. Molina, and M. J. Molina, *J. Phys. Chem. A* **103** (1999) 9042.
59. H. Y. A. Chang, T. Koop, L. T. Molina, and M. J. Molina, *J. Phys. Chem. A* **103** (1999) 2673.
60. K. Landfester, *Top. Curr. Chem.* **227** (2003) 75.
61. R. Montenegro, M. Antonietti, Y. Mastai, and K. Landfester, *J. Phys. Chem. B* **107** (2003) 5088.
62. D. J. Cziczo and J. P. D. Abbatt, *J. Geophys. Res.* **104** (1999) 13781.
63. D. J. Cziczo and J. P. D. Abbatt, *Geophys. Res. Lett.* **28** (2001) 963.
64. A. J. Prenni, M. E. Wise, S. D. Brooks, and M. A. Tolbert, *J. Geophys. Res.* **106** (2001) 3037.
65. J. H. Chelf and S. T. Martin, *J. Geophys. Res.* **106** (2001) 1215.
66. H.-M. Hung and S. T. Martin, *J. Geophys. Res.* **106** (2001) 20379.
67. H.-M. Hung, A. Malinowski, and S. T. Martin, *J. Phys. Chem. A* **106** (2002) 293.
68. H. M. Hung and S. T. Martin, *Appl. Spectrosc.* **56** (2002) 1067.
69. C. F. Braban, J. P. D. Abbatt, and D. J. Cziczo, *Geophys. Res. Lett.* **28** (2001) 3879.
70. A. J. Prenni, P. J. DeMott, S. M. Kreidenweis, D. E. Sherman, L. M. Russell, and Y. Ming, *J. Phys. Chem. A* **105** (2001) 11240.
71. D. B. Dickens and J. J. Sloan, *J. Phys. Chem. A* **106** (2002) 10543.
72. D. B. Dickens and J. J. Sloan, *J. Phys. Chem. A* **107** (2003) 9736.
73. D. H. Rasmussen, *J. Cryst. Growth* **56** (1982) 56.
74. P. J. DeMott, D. C. Rogers, and S. M. Kreidenweis, *J. Geophys. Res.* **102** (1997) 19575.
75. H. Kanno, K. Miyata, K. Tomizawa, and H. Tanaka, *J. Phys. Chem. A* **108** (2004) 6079.
76. T. Koop, *Bull. Chem. Soc. Jpn.* **75** (2002) 2587.
77. H. Kanno, R. Speedy, and C. A. Angell, *Science* **189** (1975) 880.
78. T. Koop, B. Luo, A. Tsias, and T. Peter, *Nature* **406** (2000) 611.
79. A. K. Soper, *Chem. Phys.* **258** (2000) 121.
80. R. H. Tromp, G. W. Neilson, and A. K. Soper, *J. Chem. Phys.* **96** (1992) 8460.
81. V. A. Parsegian, *Nature* **378** (1995) 335.
82. R. Leberman and A. K. Soper, *Nature* **378** (1995) 364.
83. D. H. Rasmussen, *J. Microsc.* **128** (1982) 167.
84. D. H. Rasmussen and M.-T. Liang, A theory of nucleation of ice, in *Symposium on Nucleation and Crystallization in Glasses and Liquids*, pp. 85–91, Am. Ceramic Soc., Atlanta (1993).
85. M. B. Baker and M. Baker, *Geophys. Res. Lett.* **31** (2004) in press.
86. M. Matsumoto, S. Saito, and I. Ohmine, *Nature* **416** (2002) 409.
87. S. L. Clegg, P. Brimblecombe, and A. S. Wexler, *J. Phys. Chem. A* **102** (1998) 2137.
88. Y. Zhang, C. Seigneur, J. H. Seinfeld, M. Jacobson, S. L. Clegg, and F. S. Binowski, *Atmos. Environ.* **34** (2000) 117.

89. E. C. W. Clarke and D. N. Glew, *J. Phys. Chem. Ref. Data* **14** (1985) 489.
90. B. Zobrist, U. Weers, and T. Koop, *J. Chem. Phys.* **118** (2003) 10 254.
91. B. Zuberi, *Microphysics of Atmospheric Aerosols: Phase Transitions and Cloud Formation Mechanisms*, PhD thesis, Massachusetts Institute of Technology, Cambridge (2003).
92. E. E. Dormidontova, *Macromolecules* **35** (2002) 987.
93. L. Slade and H. Levine, *Crit. Rev. Food Sci.* **30** (1991) 115.
94. T. Koop, B. Luo, U. M. Biermann, P. J. Crutzen, and T. Peter, *J. Phys. Chem. A* **101** (1997) 1117.
95. H. R. Pruppacher, *J. Atmos. Sci.* **52** (1995) 1924.
96. Y. S. Djikaev, A. Tabazadeh, P. Hamill, and H. Reiss, *J. Phys. Chem. A* **106** (2002) 10 247.
97. A. Tabazadeh, Y. S. Djikaev, P. Hamill, and H. Reiss, *J. Phys. Chem. A* **106** (2002) 10 238.
98. A. Tabazadeh, Y. S. Djikaev, and H. Reiss, *Proc. Nat. Acad. Sci. USA* **99** (2002) 15 873.
99. P. Stöckel, H. Vortisch, T. Leisner, and H. Baumgärtel, *J. Mol. Liq.* **96–97** (2002) 153.
100. D. Duft and T. Leisner, *Atmos. Chem. Phys. Disc.* **4** (2004) 3077.
101. R. A. Shaw and D. Lamb, *Geophys. Res. Lett.* **26** (1999) 1181.
102. M. Gavish, R. Popovitz-Biro, M. Lahav, and L. Leiserowitz, *Science* **250** (1990) 973.
103. D. J. Bowles, P. J. Lillford, D. A. Rees, and I. A. Shanks (Eds.), *Coping with the cold: the molecular and structural biology of cold stress survivors*, vol. B 357, pp. 829–955 of *Phil. Trans. R. Soc. Lond.* (2002).
104. K. E. Zachariassen and E. Kristiansen, *Cryobiology* **41** (2000) 257.
105. D. H. Rasmussen, M. N. MacAulay, and A. P. MacKenzie, *Cryobiology* **12** (1975) 328.
106. B. Kärcher and U. Lohmann, *J. Geophys. Res.* **108** (2003) 4402, doi:10.1029/2002JD003220.
107. P. W. Wilson, A. F. Heneghan, and A. D. J. Haymet, *Cryobiology* **46** (2003) 88.
108. C. Gable, H. Betz, and S. Maron, *J. Am. Chem. Soc.* **72** (1950) 1445.
109. R. Zhang, *Laboratory investigations of heterogeneous chemistry important to ozone depletion in the stratosphere*, PhD thesis, Massachusetts Institute of Technology, Cambridge (1993).
110. K. Beyer, *Laboratory experiments of chemical reactions on PSC particles*, PhD thesis, Massachusetts Institute of Technology, Cambridge (1994).
111. K. Ji, *Etudes de la compositions des aerosols stratosphériques polaires au moyen des diagrammes de phase stables, metastables et cinétiques des systems: HNO₃/H₂O, HCL/H₂O et H₂SO₄/H₂O*, PhD thesis, L'université de Paris, Paris (1994).
112. T. Koop, *Die Bildungsmechanismen von Polaren Stratosphärenwolken*, PhD thesis, Johannes Gutenberg-Universität, Mainz (1996).
113. G. Vuillard, *Bull. Soc. Chim.* **1954** (1954) 802.
114. H. Kanno and H. Itoi, *Ryusan to Kogyo* **37** (1984) 181.
115. B. Zobrist, *Untersuchungen zum Gefrierverhalten von wässrigen Polyethylenglykol-Lösungen mit einem selbstentwickelten Kalorimeter*, Diploma thesis, ETH Zürich, Zurich, Switzerland (2001).
116. K. Miyata, H. Kanno, K. Tomizawa, and Y. Yoshimura, *Bull. Chem. Soc. Jpn.* **74** (2001) 1629.
117. O. Mishima, *Nature* **384** (1996) 546.
118. H. Kanno and C. A. Angell, *J. Phys. Chem.* **81** (1977) 2639.